Experimental Study of Effects of GO-SiO_2-TiO_2–SDS Hybrid Nanofluids on Interfacial Tension by Du Noüy Ring Method

Pourabdol Shahrekordi, Arash
Department of Petroleum Engineering, Faculty of Petroleum and Chemical Engineering, Science and Research Branch, Islamic Azad University, Tehran, I.R. IRAN

Sheikh Zakariaei, Seyed Jamal
Department of Earth Sciences, Faculty of Converging Science and Technologies, Science and Research Branch, Islamic Azad University, Tehran, I.R. IRAN

Zargar, Ghasem*[*+]*; Khaksar Manshad, Abbas
Department of Petroleum Engineering, Abadan Faculty of Petroleum Engineering, Petroleum University of Technology (PUT), Abadan, I.R. IRAN

ABSTRACT: *This research aimed to prepare and utilize a novel hybrid nanofluid (GO-SiO_2-TiO_2–SDS) to significantly reduce the InterFacial Tension (IFT) to a level lower than the IFT value of the SDS surfactant solution at the Critical Micelle Concentration (CMC) point. Accordingly, the GO-SiO_2-TiO_2 nanocomposite was synthesized, and its properties were evaluated through six different analyses, including Field Emission Scanning Electron Microscopy (FESEM), Energy Dispersive X-ray Spectroscopy (EDXS), Map Analysis, Fourier Transform InfraRed (FT-IR), spectroscopy X-Ray Diffraction (XRD), and ThermoGravimetric Analysis (TGA). To assess the effects of GO-SiO_2-TiO_2–SDS hybrid nanofluids on IFT reduction, SDS surfactant solutions were prepared at varying concentrations of SDS (0, 200, 500, 1000, 2000, 3000, 4000, 5000, and 6000 ppm), and 500 ppm was determined as the CMC. Different concentrations of the GO-SiO_2-TiO_2 nanocomposite (100, 500, 1500, and 2500 ppm) were separately added to deionized water, and then the SDS surfactant was added at the CMC value to prepare hybrid nanofluids. The results of IFT measurements reported by the Du Noüy ring method indicated that IFT values at the interfaces between 500-ppm SDS surfactant solution/kerosene and (2500 ppm GO-SiO_2-TiO_2–500 ppm SDS) hybrid nanofluid/kerosene decreased from 23.59 mN/m to 2.48 mN/m and 0.51 mN/m, respectively. Therefore, using the GO-SiO_2-TiO_2–SDS hybrid nanofluid could reduce the IFT value to a level lower than that of the SDS surfactant solution at the CMC point.*

KEYWORDS: *Hybrid nanofluids, GO-SiO_2-TiO_2 nanocomposite, SDS surfactant, Interfacial tension reduction, Du Noüy ring method.*

* *To whom correspondence should be addressed.*
+ E-mail: zargar@put.ac.ir
1021-9986/2023/11/3598-3610 13/$/6.03

INTRODUCTION

Nanotechnology is now considered an extremely hot and intriguing topic [1]. With the ever-increasing need for energy worldwide, the use of this technology in different energy-related industries, such as the oil industry, has become increasingly important [2]. An application of nanotechnology in the petroleum industry is to employ nanocomposite-surfactant hybrid nanofluids to further reduce InterFacial Tension (IFT) and release or produce more crude oil trapped in reservoir pores (i.e., the residual oil). However, all previous research projects have only used two-component nanocomposites. In fact, they have never applied three-component nanocomposites such as the one synthesized for the first time in this research project to prepare IFT-reducing nanocomposite-surfactant hybrid nanofluids. Compared with two-component nanocomposites, the advantage of using three-component nanocomposites in preparing IFT-reducing nanocomposite-surfactant hybrid nanofluids would be to provide certain conditions in which the IFT-reducing characteristics of three nanomaterials could be employed to help the surfactant to further reduce IFT.

In fact, IFT is a factor that traps a large amount of crude oil as residual oil in reservoir pores. This residual oil can be released and produced by using IFT-reducing agents such as surface-active agents (surfactants) and various nanoparticles (e.g., SiO_2, TiO_2, Al_2O_3, ZrO_2, Fe_2O_3, and GO) [3, 4, 5, 6, 7]. The foregoing methods are classified as the chemical techniques of oil recovery and are considered a subset of tertiary recovery methods (EOR methods). In general, surfactants and nanoparticles cause one liquid to disperse in another liquid and form emulsions through absorption to the interface between two immiscible liquids (e.g., water and oil). Therefore, they reduce IFT, capillary forces, and the volume of residual oils in the reservoir. Many researchers have tested the idea of using surfactants and nanoparticles simultaneously as nanoparticle-surfactant hybrid nanofluids to improve the efficiency of surfactants in further IFT reductions. For instance, *Mohajeri et al.* analyzed the effects of the ZrO_2-SDS hybrid nanofluid and the SDS surfactant solution on IFT reduction. They reported that ZrO_2-SDS hybrid nanofluid and SDS surfactant solution reduced IFT by 3.1 and 16 mN/m, respectively [8]. Likewise, *Tavakkoli et al.* reported that SDS surfactant solutions and Al_2O_3-SDS hybrid nanofluids could reduce IFT by 3 and 0.8 mN/m, respectively [9]. Some other researchers tested the idea of using nanocomposites instead of nanoparticles to further decrease IFT. For example, *Kazemzadeh et al*. observed that SiO_2, TiO_2, and TiO_2-SiO_2 nanofluids reduced IFT by 16.8, 19.1, and 13.2 mN/m, respectively [10]. Recently, researchers have integrated the two foregoing ideas in their research projects to further reduce IFT. In other words, they have used nanocomposite-surfactant hybrid nanofluids for this purpose. According to *Garmroudi et al*., the hybrid nanofluids of the GO-TiO_2 and ZSCL extract and those of the GO and ZSCL extract decreased IFT by 10.5 and 12.3 mN/m, respectively. They concluded that nanocomposite-surfactant hybrid nanofluids were more efficient than nanoparticle-surfactant hybrid nanofluids in reducing IFT [11]. Table 1 presents an overview of previous research projects on IFT reduction through the use of nanocomposite-surfactant hybrid nanofluids. In this research, the GO-SiO_2-TiO_2 nanocomposite, a nanocomposite based on three different IFT-reducing nanomaterials, was synthesized for the first time. This nanocomposite was then used to prepare GO-SiO_2-TiO_2–SDS hybrid nanofluids at different nanocomposite concentrations and the surfactant CMC value. The preparation of GO-SiO_2-TiO_2–SDS hybrid nanofluids led to the creation of a new category called the IFT-reducing nanocomposite-surfactant hybrid nanofluids based on the three-component nanocomposites. These nanofluids were evaluated and studied experimentally for the first time in this research. Moreover, GO-SiO_2-TiO_2–SDS hybrid nanofluids were prepared for the following purposes: (i) simultaneous use of the IFT-reducing characteristics of the three-component nanocomposite and the surfactant, (ii) measuring the IFT values between the prepared GO-SiO_2-TiO_2–SDS hybrid nanofluids at different concentrations of the nanocomposite and kerosene, and (iii) determining the best nanocomposite concentration in the hybrid nanofluid that can minimize the IFT value.

EXPERIMENTAL SECTION

Materials

For research purposes, GO nanomaterials with a thickness of 3.4-7 nm and purity of more than 99%, as well as anatase-TiO_2 nanomaterials with a thickness of 10-25 nm and purity of 99.5%, were purchased from the US Research Nanomaterials Company. Fig.s 1 and 2 display their FESEM images. Deionized water, absolute ethanol

Table 1: An overview of research projects on IFT reduction through using nanocomposite–surfactant hybrid nanofluids

IFT (mN/m)		Base fluid	Nanocomposite		Reference
To	From		Concentration (ppm)	type	
0.18	29.1	Surfactant solution (CTAB + Brine)	500	Fe_3O_4-Eggshell	Omidi et al. [12]
2.4	27	Surfactant solution (CP plant extract + DDW)	250	ZnO-MMT	Nourinia et al. [13]
1.354	29.18	Surfactant solution (DTAB + Distilled water)	1000	ZnO-PAM	Asl et al. [14]

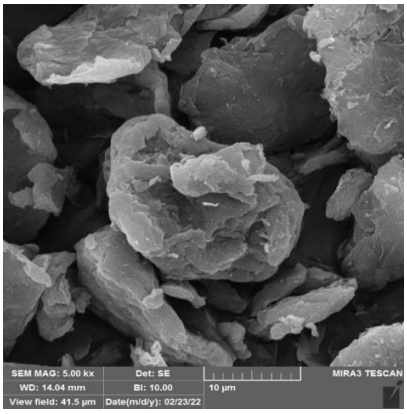

Fig. 1: FESEM image of GO nanomaterial

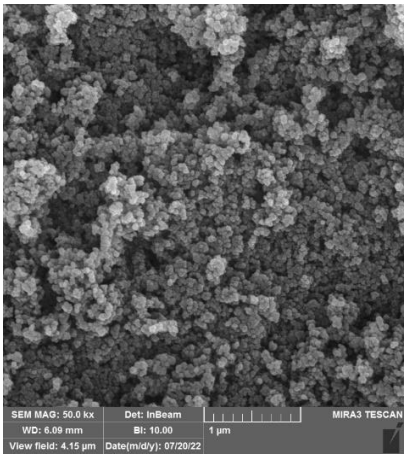

Fig. 2: FESEM image of anatase-TiO_2 nanomaterial

(C_2H_5OH, 99.9%),tetraethyl orthosilicate (TEOS, 98%), ammonia solution (NH_4OH, 25%), and SDS (85%) surfactant were all purchased from Merck Company.

Additionally, kerosene was supplied by Shiraz Oil Refining Company. Deionized water was utilized in the process of synthesizing nanocomposites, preparing surfactant solutions, and as the base fluid to prepare nanocomposite-surfactant nanofluids. Furthermore, kerosene was employed as the oil phase.

Research flowchart

Fig. 3 represents the stepwise flowchart of all experiments conducted in this research from the first experiment to the last one.

Synthesis of GO-SiO_2-TiO_2 Nanocomposite

The synthesis process of GO-SiO_2-TiO_2 nanocomposite powder consisted of two stages. In the first stage, the GO-SiO_2 nanocomposite was synthesized through the in-situ hydrolysis and condensation of TEOS on the surfaces of GO nanosheets. For this purpose, 0.05 g of GO nanomaterial, 150 mL of absolute ethanol, and 30 mL of deionized water were stirred with a magnetic stirrer for 35 minutes at 1500 rpm to create a mixture. To homogenize the mixture and separate GO nanosheets, the mixture was then placed in an ultrasonic bath (Falc LBS2 device, 4.5 liters) with an ultrasonic frequency of 40 kHz for one hour. Afterward, a solution of ammonia was added dropwise to the mixture to adjust the pH to 9, and 0.8 mL of TEOS was used as a source of silica and added dropwise to the mixture. The resultant mixture was again placed in an ultrasonic bath for 40 minutes with an ultrasonic frequency of 40 kHz. The final mixture was placed at room temperature for 24 hours to complete the reaction and form GO-SiO_2 nanocomposite suspension (Fig. 4). Eventually, the solid content of the suspension (i.e., GO-SiO_2 nanocomposite) was separated through centrifugation, washed three times With absolute ethanol and once with deionized water, and placed in 15 mL of absolute ethanol.

The hydrothermal method was used in the second stage of GO-SiO_2-TiO_2 nanocomposite synthesis. For this purpose, 35 mL of deionized water was added to the mixture of the GO-SiO_2 nanocomposite and absolute ethanol. Then, 0.46 g of the anatase-TiO_2 nanomaterial was added to the mixture, and the resultant mixture was stirred for two hours at 1500 rpm to obtain a completely uniform mixture in terms of color. The homogenized mixture was then placed in an autoclave

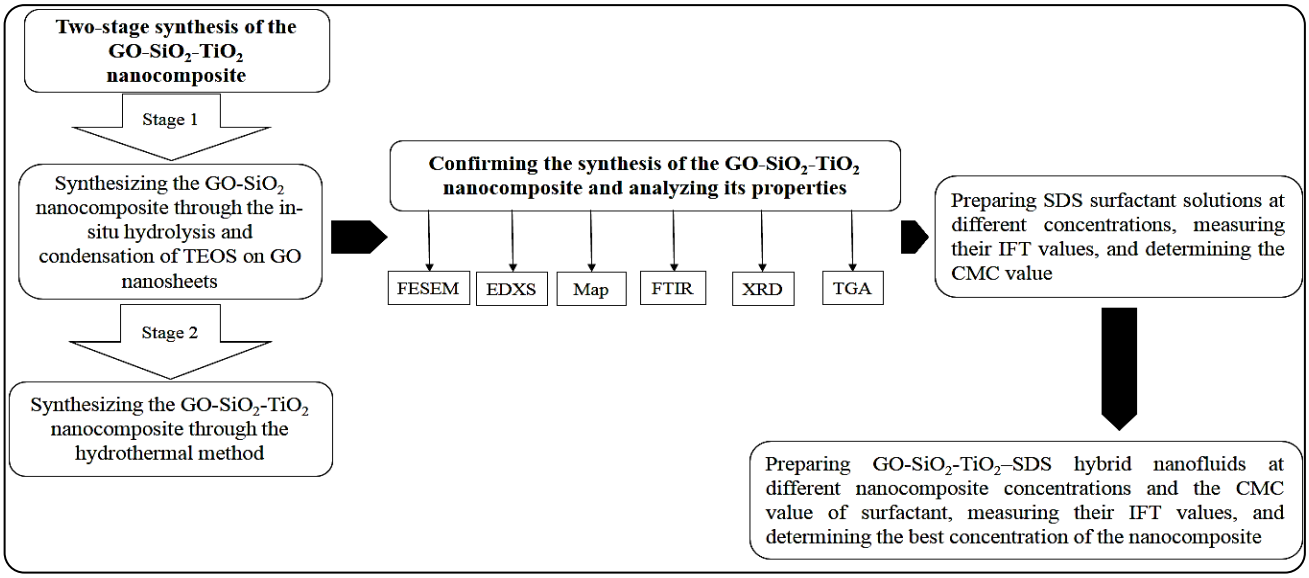

Fig. 3: The flowchart of this research

Fig. 4: GO-SiO2 nanocomposite suspension

Fig. 5: GO-SiO2-TiO2 nanocomposite powde

for six hours at 120 °C. Eventually, the final product (the GO-SiO_2-TiO_2 nanocomposite) was separated through centrifugation, washed three times with absolute ethanol and once with deionized water, and dried at room temperature to turn into powder (Fig. 5).

Confirmation of Nanocomposite Synthesis and Analysis of its Properties

Six different analyses were conducted to confirm the synthesis of the GO-SiO_2-TiO_2 nanocomposite and evaluate its properties. They were field emission scanning electron microscopy (FESEM, by the Tescan Mira3 device), energy dispersive X-ray spectroscopy (EDXS), map analysis, Fourier-transform infrared spectroscopy (FT-IR, by the Thermo Scientific-Nicolet iS10 device), X-ray diffraction (XRD, by the Philips PW1730 device), and thermogravimetric analysis (TGA, by the SDT-Q600 device).

Preparation of surfactant solutions and Nanocomposite-surfactant Nanofluids

The Critical Micelle Concentration (CMC) point of the surfactant, at which the lowest IFT is observed, was defined as the concentration at which surfactant molecules start to aggregate and form micelles [15]. The CMC point is an important factor when using surfactants alone as surfactant solutions or mixed with nanomaterials or nanocomposites as hybrid nanofluids. Surfactant solutions were prepared at different concentrations to determine the CMC point of the surfactant. Therefore, different concentrations of the SDS surfactant (i.e., 0, 200, 500, 1000,

Fig. 6: Sigma 703D force tensiometer device employed to measure IFT values

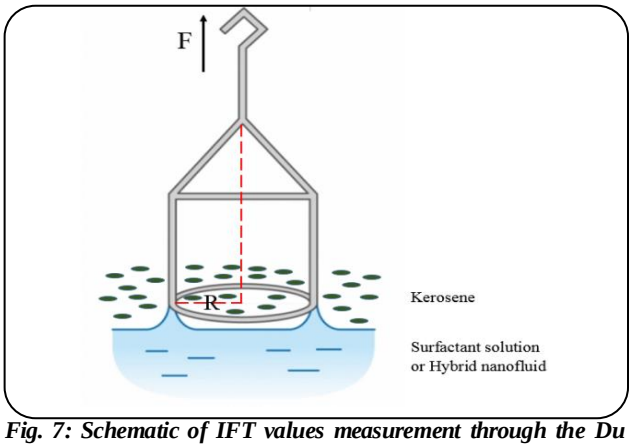

Fig. 7: Schematic of IFT values measurement through the Du Noüy ring method used in the Sigma 703D force tensiometer device

2000, 3000, 4000, 5000, and 6000 ppm) were separately added to deionized water and stirred with a magnetic stirrer at low speed (to avoid the formation of foam) for five minutes. This process resulted in the preparation of colorless SDS surfactant solutions at different concentrations. The CMC point of the SDS surfactant was then determined, followed by separately adding different concentrations of the GO-SiO_2-TiO_2 nanocomposite (i.e., 100, 500, 1500, and 2500 ppm) to deionized water to prepare nanofluids at different concentrations of the nanocomposite. Next, they were exposed to ultrasound waves for 30 minutes using an ultrasonic homogenizer (i.e., Sigma Sonic UH-1200-20 device) running at 70% power to ensure that nanocomposite particles were thoroughly dispersed in the deionized water. The SDS surfactant was then added to the nanofluids at the CMC value and stirred with a magnetic stirrer at low speed for five minutes. This process resulted in the preparation of nanocomposite-surfactant hybrid nanofluids at different concentrations of the nanocomposite and the CMC value of the surfactant.

Table 2: The weight and atomic percentages of the constituents of GO-SiO_2-TiO_2 nanocomposite

Elements	Wt. %	At. %
C	4.47	9.31
O	38.41	60.02
Si	2.31	2.06
Ti	54.81	28.61

Measurement of IFT Values

The Sigma 703D force tensiometer device was used to measure the IFT values between the surfactant solutions or hybrid nanofluids at different concentrations and kerosene in ambient conditions (Fig. 6). The device utilizes the Du Noüy ring method to measure IFT values. To this end, half of the glass container of the device was filled with a surfactant solution or hybrid nanofluid, while the other half was filled with kerosene. The thin platinum ring of the device was then placed vertically under the interface between the two liquids and gradually brought up. The device measured the force required to separate the ring from the interface between the two liquids (Fig. 7) and calculated the IFT value using Eq. (1).

$$\sigma = \frac{F}{4\pi r} f \quad (1)$$

Where σ and F denote the IFT and the force required to separate the ring from the interface between two liquids (i.e., the surfactant solution or hybrid nanofluid and kerosene), respectively, moreover, r and f represent the ring radius and the correction coefficient, respectively.

RESULTS AND DISCUSSION

Results of FESEM, EDXS, and map analyses

Fig. 8 shows the FESEM images of the GO-SiO_2-TiO_2 nanocomposite at five different scales (i.e., 10 µm, 5 µm, 2 µm, 500 nm, and 200 nm). Additionally, Fig. 9 depicts the presence of carbon (C), oxygen (O), silicon (Si), and titanium (Ti) in the nanocomposite. Table 2 lists the weight and atomic percentages of these elements in the nanocomposite. Fig. 10 illustrates the distribution and

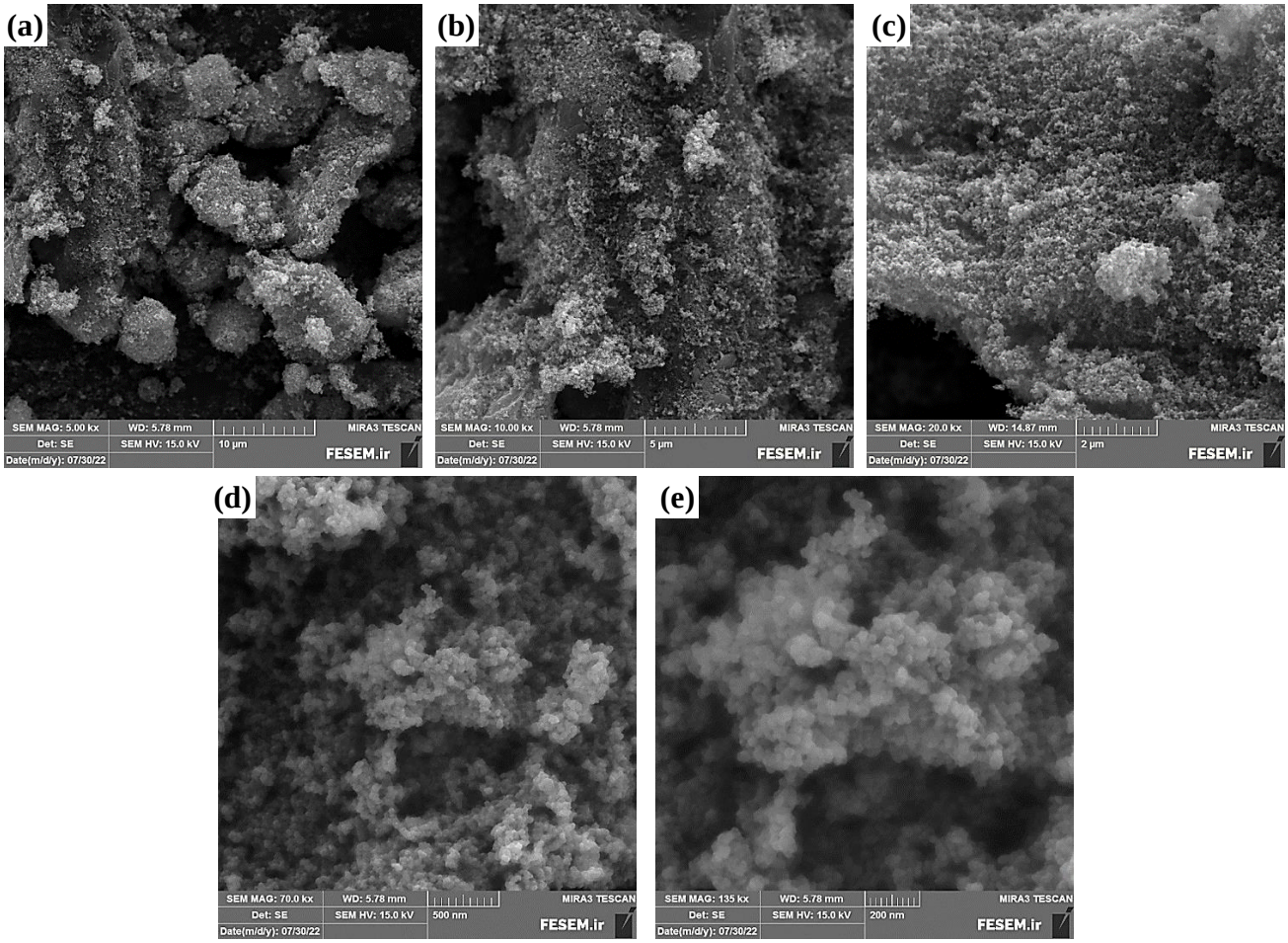

Fig. 8: The FESEM images of GO-SiO_2-TiO_2 nanocomposite on five different scales: a) 10 µm, b) 5 µm, c) 2 µm, d) 500 nm, and e) 200 nm

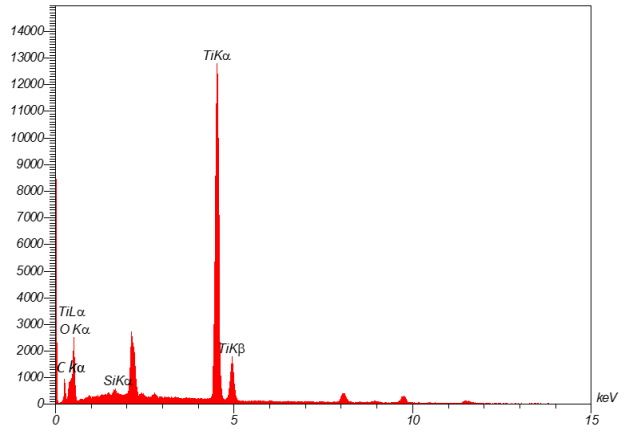

Fig. 9: EDXS analysis of GO-SiO_2-TiO_2 nanocomposite

dispersion of C, O, Si, and Ti elements in both separate and combined forms within the GO-SiO_2-TiO_2 nanocomposite. Furthermore, the distribution maps of Si and Ti elements on GO nanosheets in this nanocomposite indicate that Si and Ti are uniformly distributed and dispersed on the nanosheets.

Results of FT-IR analysis

The chemical bonds of the GO-SiO_2-TiO_2 nanocomposite were assessed using the FT-IR analysis, and Fig. 11 displays the FT-IR spectrum of the nanocomposite.

The spectrum exhibits various peaks, including the peak at 3416.70 cm^{-1}, which is due to the stretching vibration of the O–H bonds of adsorbed water molecules and hydroxyl groups on the surface of GO nanosheets [16]. Additionally, the peak at 2921.77 cm^{-1} corresponds to the stretching vibration of C–H bonds at the edges and defect zones of GO nanosheets [17, 18]. The peak centered at 2368.27 cm^{-1} results from the presence of carbon dioxide gas in the FT-IR chamber [19]. Moreover, the peaks centered at 1697.13 and 1629.63 cm^{-1} correspond to the stretching vibration of C=O bonds in carboxylic groups at the edges of GO nanosheets and the stretching vibration of C=C bonds in aromatic rings of this nanomaterial, respectively [20, 21]. The peak located at 1384.70 cm^{-1} can be attributed to the bending vibration of C–H bonds in the GO

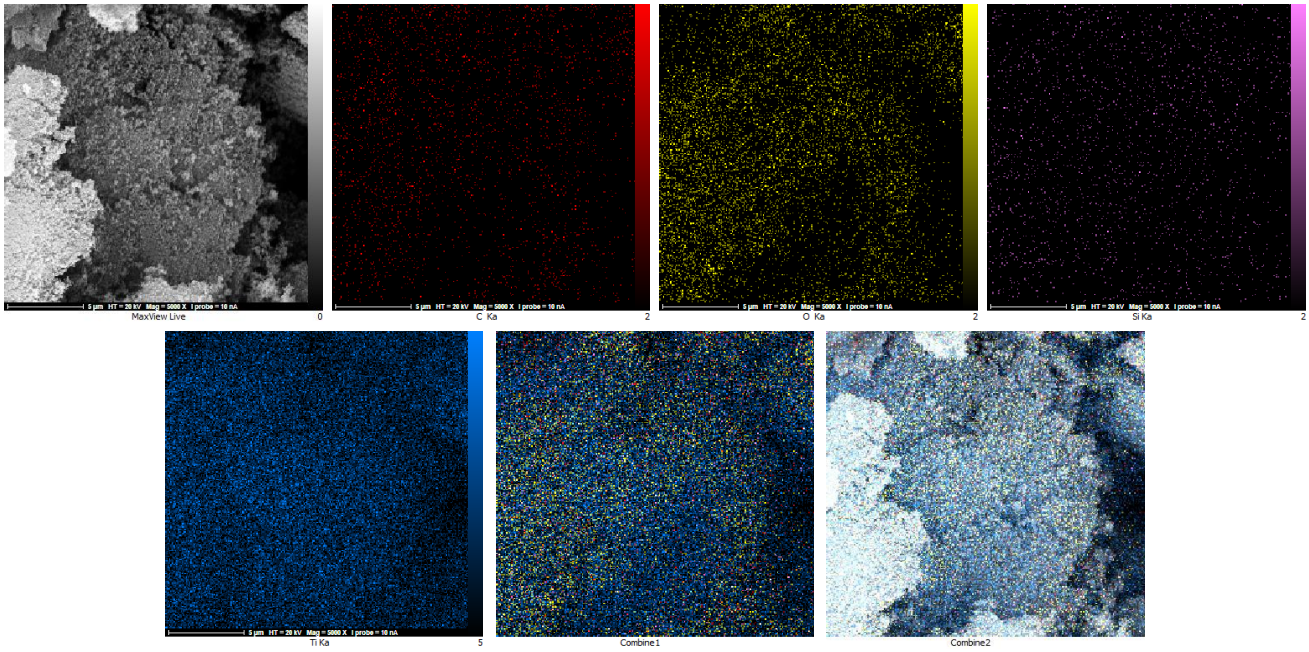

Fig. 10: The distribution maps of constituents of GO-SiO_2-TiO_2 nanocomposite

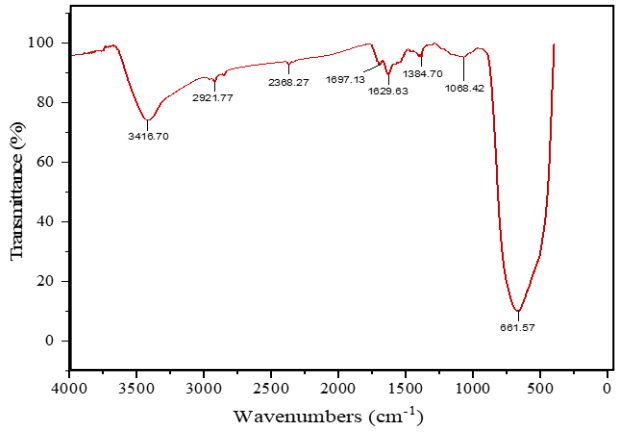

Fig. 11: The FT-IR spectrum of the GO-SiO_2-TiO_2 nanocomposite

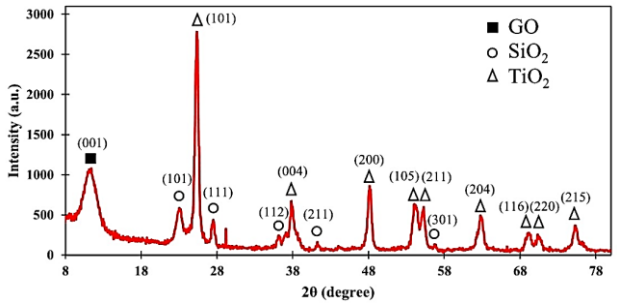

Fig. 12: The XRD pattern of the GO-SiO_2-TiO_2 nanocomposite

nanosheet structure [22]. Furthermore, the peak at 1068.42 cm^{-1} is caused by the symmetric stretching vibration of the Si-O-Si group in the SiO_2 nanomaterial [23, 24], and the peak at 661.57 cm^{-1} is assigned to the stretching vibration of Ti–O bonds in the TiO_2 nanomaterial's structure [25,26]. Thus, the FT-IR analysis confirms the presence of SiO_2 and TiO_2 nanomaterials, along with GO nanosheets.

Results of XRD Analysis

After conducting XRD analysis on the GO-SiO_2-TiO_2 nanocomposite, X'Pert HighScore Plus was utilized to identify crystalline phases present in the nanocomposite. The results of the analysis revealed the presence of three different phases. As depicted in Fig. 12, the broad peak observed at 11.4° corresponds to the (001) diffraction plane of GO nanosheets [27, 28, 29]. Additionally, the peak located at 23.0° can be considered the characteristic peak of the SiO_2 nanomaterial, specifically the cristobalite phase with a tetragonal crystalline structure and a space group of P41212 (Reference code: JCPDS No. 01-076-0941) [30, 31, 32]. The diffraction planes of silica at (101), (111), (112), (211), and (301) were located at 2θ= 23.0°, 27.5°, 36.1°, 41.2°, and 56.2°, respectively. Furthermore, anatase-TiO_2 was detected as a crystalline phase with a tetragonal crystalline structure and a space group of I41/amd (Reference code: JCPDS No. 00-021-1272). The diffraction planes of anatase-TiO_2 at (101), (004), (200), (105), (211), (204), (116), (220), and (215) were located at 2θ= 25.3°, 37.8°, 48.2°, 54.0°, 55.3°, 62.9°, 69.4°, 70.5°,

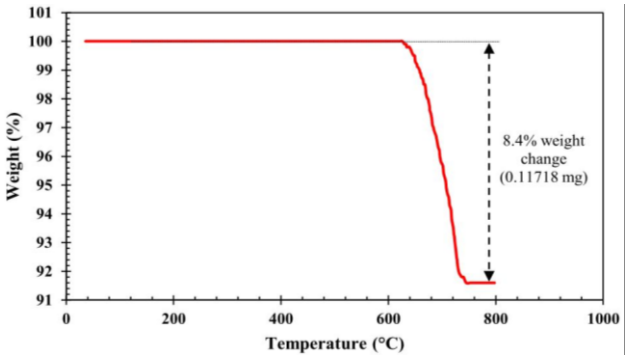

Fig. 13: The TGA thermogram of the GO-SiO_2-TiO_2 nanocomposite

and 75.5°, respectively. Therefore, based on the XRD analysis, the GO-SiO_2-TiO_2 nanocomposite contains GO, SiO_2, and anatase-TiO_2 phases.

Results of TGA

The TGA was conducted on 1.3950 mg of the nanocomposite in an argon atmosphere with a heating rate of 10 °C/minute to evaluate the thermal stability of the GO-SiO_2-TiO_2 nanocomposite.

According to Fig. 13, the thermal decomposition of the nanocomposite started at 626 °C and continued up to 745 °C. Based on the results, 8.4 wt.% (0.11718 mg) of the nanocomposite was decomposed within this temperature range. The nanomaterials of SiO_2 and TiO_2 existing in the nanocomposite cannot be decomposed within the mentioned temperature range since they remain stable until 800 °C [33, 34]. Therefore, the weight loss in this temperature range is due to dihydroxylation from the surfaces of GO nanosheets existing in the nanocomposite and the thermal decomposition (pyrolysis) of the carbon skeleton in the GO present in the nanocomposite [35, 36]. According to the TGA results reported by *Haeri et al*. [37] and Ramezanzadeh et al. [38], the starting temperature of the thermal decomposition of the GO-SiO_2 nanocomposite was higher than that of the pure GO nanomaterial. This temperature difference is due to the presence of silica nanomaterials on the surface of GO nanosheets. The TGA results of the GO-SiO_2 nanocomposites in those studies were compared with the results of the GO-SiO_2-TiO_2 nanocomposite in the present study. The comparison indicated that the starting temperature of the thermal decomposition of the GO-SiO_2-TiO_2 nanocomposite was significantly higher than that of the GO-SiO_2 nanocomposite. This significant difference is due to the presence of TiO_2 nanomaterials in addition to the presence of SiO_2 nanomaterials in the GO-SiO_2-TiO_2 nanocomposite structure. Hence, the presence of SiO_2 and TiO_2 nanomaterials in the structure of the GO-SiO_2-TiO_2 nanocomposite had a significantly positive effect on increasing the thermal stability of this nanocomposite.

Table 3: Changes in IFT values due to changes in SDS concentrations in surfactant solutions

SDS concentration in surfactant solution (ppm)	IFT (mN/m)	Explanation
0	23.59	Deionized Water
200	3.16	
500	2.48	CMC point
1000	3.94	
2000	4.28	
3000	4.17	
4000	4.36	
5000	4.42	
6000	3.7	

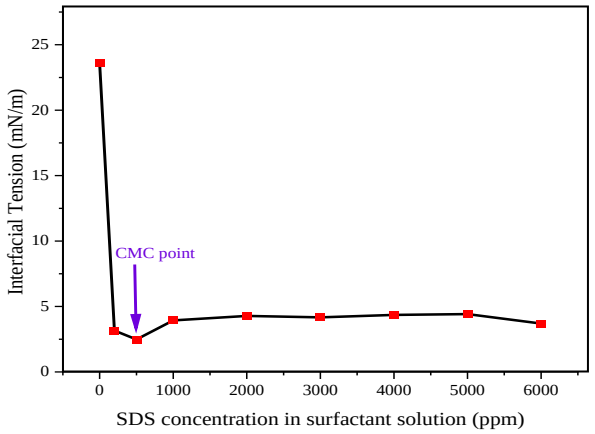

Fig. 14: The graph of changes in IFT values due to changes in SDS concentrations in surfactant solutions (based on Table 3)

Measurement of IFT values

Table 3 and Fig. 14 demonstrate the measured IFT values at interfaces between SDS surfactant solutions with different concentrations (0, 200, 500, 1000, 2000, 3000, 4000, 5000, and 6000 ppm) and kerosene. As the concentration of the SDS surfactant increased from 0 to 500 ppm, the IFT value sharply decreased to a minimum level. This implies that the 500-ppm concentration of the SDS surfactant, which resulted in the minimum IFT level (2.48 mN/m), was the CMC point of the surfactant. However, the IFT value increased as the surfactant concentration increased from 500 to 1000 ppm. As the concentration further

Table 4: Research hypotheses

Number	Hypothesis
1	Using the GO-SiO_2-TiO_2–SDS hybrid nanofluid can reduce the IFT value to a lower level than the IFT value of the SDS surfactant solution at the CMC point.
2	Using the GO-SiO_2-TiO_2–SDS hybrid nanofluid can significantly reduce the IFT value.

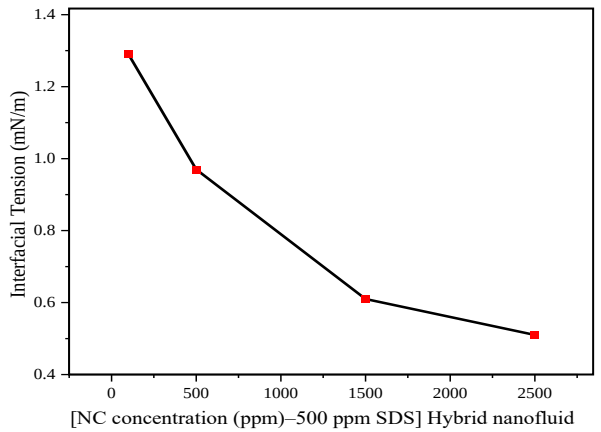

Fig. 15: Changes in IFT values due to changes in nanocomposite concentrations in hybrid nanofluids (based on Table 4)

Fig. 16: (2500 ppm GO-SiO_2-TiO_2–500 ppm SDS) Hybrid nanofluid

Table 5: Changes in IFT values due to changes in nanocomposite concentrations in hybrid nanofluids

[NC concentration (ppm)–500 ppm SDS] Hybrid nanofluid	IFT (mN/m)
100	1.29
500	0.97
1500	0.61
2500	0.51

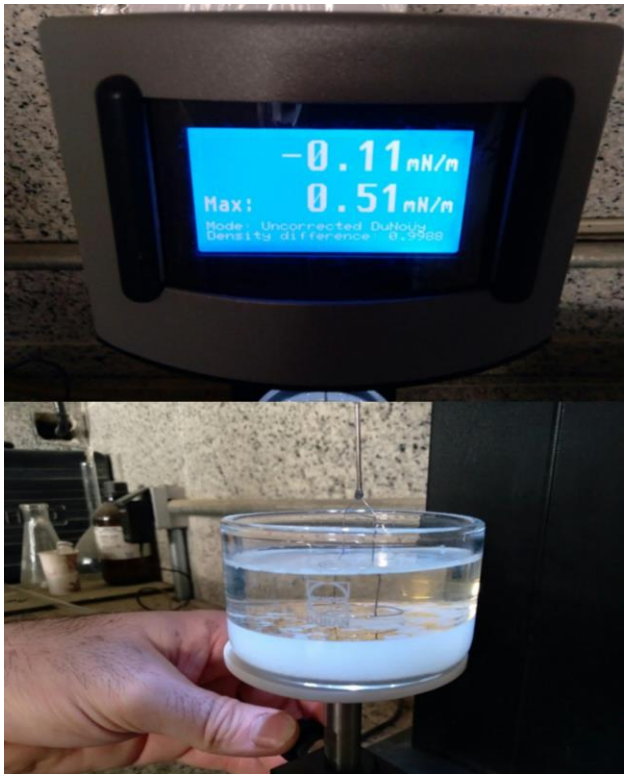

Fig. 17: Measurement of IFT value for (2500 ppm GO-SiO_2-TiO_2–500 ppm SDS) hybrid nanofluid

increased from 1000 to 6000 ppm, the IFT value became almost uniform with slight changes and small fluctuations.

After considering the 500-ppm concentration of the SDS surfactant as the CMC point, GO-SiO_2-TiO_2–500 ppm SDS hybrid nanofluids were prepared at different concentrations of the GO-SiO_2-TiO_2 nanocomposite (i.e., 100, 500, 1500, and 2500 ppm) to analyze research hypotheses (Table 4). The IFT values at the interfaces between hybrid nanofluids and kerosene were then measured (Table 5 & Fig. 15), and the results revealed that an increase in the concentration of the GO-SiO_2-TiO_2 nanocomposite in the hybrid nanofluid from 100 to 2500 ppm resulted in a continuous decrease in the IFT value. At all the mentioned concentrations of the nanocomposite, The measured IFT values were lower than the IFT value at the nanocomposite concentration of 0 ppm (i.e., the SDS surfactant solution at the CMC point). This finding confirmed Hypothesis 1 in this research project. In addition, the lowest IFT value of 0.51 mN/m was recorded at the 2500-ppm concentration of the nanocomposite in the hybrid nanofluid (Figs. 16 and 17). Hence, the IFT value was significantly reduced to the lowest level when the hybrid nanofluid was used with a 2500-ppm nanocomposite concentration. This finding confirmed Hypothesis 2 in the current research. According to Fig. 17, the interface between the hybrid nanofluid with a nanocomposite concentration of 2500 ppm and kerosene became unstable because it had the lowest IFT value.

The hybrid nanofluid with a 100-ppm concentration of the nanocomposite could significantly reduce the IFT value from 2.48 mN/m (i.e., the IFT value of the SDS surfactant solution at the CMC point) to 1.29 mN/m. This was because the nanocomposites that absorbed many surfactant molecules on their surfaces moved to the interface between the hybrid nanofluid and kerosene by Brownian motion [39, 40]. As a result, an additional amount of surfactant molecules emerged on the interface, which further reduced the IFT value [9]. There was also a downward trend in the IFT value when the nanocomposite concentration in the hybrid nanofluid increased from 100 ppm to 2500 ppm. In fact, the IFT value finally reached 0.51 mN/m (i.e., the IFT value at a 2500-ppm concentration of the nanocomposite) because increasing the nanocomposite concentration in the hybrid nanofluid increased the number of nanocomposites absorbed to the interface. Accordingly, further nanocomposites appeared on the interface. Given the IFT-reducing characteristics of this nanocomposite, its abundance in the presence of surfactant molecules could further decrease the IFT value [11].

CONCLUSIONS

This study sought to investigate the effects of GO-SiO_2-TiO_2–SDS hybrid nanofluids on the reduction of IFT under laboratory conditions. The experiments conducted in this research project involved various steps, including the synthesis of the nanocomposite, the confirmation of nanocomposite synthesis and characterization of its properties, the preparation of surfactant solutions and nanocomposite-surfactant hybrid nanofluids, and the measurement of IFT values using the Du Noüy ring method.

The results of the experiments revealed several key findings. First, the synthesis of the GO-SiO_2-TiO_2 nanocomposite and its properties was confirmed and evaluated using various analytical techniques such as FESEM, EDXS, Map, FT-IR, XRD, and TGA analyses. In addition, the CMC value of the SDS surfactant was determined to be 500 ppm. Further, the use of the SDS surfactant solution at the CMC value of 500 ppm significantly decreased the IFT value from 23.59 to 2.48 mN/m.

Moreover, the use of GO-SiO_2-TiO_2–SDS hybrid nanofluids at all nanocomposite concentrations (i.e., 100, 500, 1500, and 2500 ppm) resulted in a reduction in IFT values to levels lower than the IFT value of the SDS surfactant solution at the CMC point. Specifically, using the hybrid nanofluid with a concentration of 2500 ppm GO-SiO_2-TiO_2 and 500 ppm SDS led to the lowest IFT value of 0.51 mN/m, which was significantly lower than the IFT value of the SDS surfactant solution at the CMC point.

Overall, the findings suggest that GO-SiO_2-TiO_2–SDS hybrid nanofluids have great potential for reducing IFT values.

Acknowledgments

The authors would like to express their appreciation for the valuable guidance provided by Dr. Farzaneh Ebrahimzadeh, the Assistant Professor of Organic Chemistry at the Islamic Azad University of Marvdasht Branch, which enabled the synthesis of the analyzed nanocomposite in this research project.

Nomenclature

Aluminum oxide	Al_2O_3
Critical micelle concentration	CMC
Cyclamen persicum	CP
Cetyl trimethyl ammonium bromide	CTAB
Double deionized water	DDW
Dodecyl trimethyl ammonium bromide	DTAB
Energy dispersive X-ray spectroscopy	EDXS
Enhanced oil recovery	EOR
Force required to separate the ring from the interface between two liquids, mN	F
Correction coefficient, dimensionless	f
Iron(III) oxide	Fe_2O_3
Field emission scanning electron microscopy	FESEM
Fourier transform infrared spectroscopy	FT-IR
Graphene oxide	GO
Interfacial tension	IFT
Montmorillonite	MMT
Polyacrylamide	PAM
parts per million	ppm
Radius of the ring, m	r
Sodium dodecyl sulfate	SDS
Silica	SiO_2
Tetraethyl Orthosilicate	TEOS
Thermogravimetric analysis	TGA
Titanium oxide	TiO_2
X-ray diffraction	XRD
Zinc oxide	ZnO
Zirconium oxide	ZrO_2
Ziziphus spina-christi leaf	ZSCL
Interfacial tension, mN/m	σ

Received: Mar. 23, 2023; Accepted: Jun. 26, 2023

REFERENCES

[1] Chamkha A.J., Armaghani T., Mansour M.A., Rashad A.M., Kargarsharifabad H., MHD Convection of an Al_2O_3-Cu/Water Hybrid Nanofluid in an Inclined Porous Cavity with Internal Heat Generation/Absorption, *Iran. J. Chem. Chem. Eng. (IJCCE)*, **41(3):** 936-956 (2022).

[2] Ghorbany M., Abedini A., Kargarsharifabad H., A Numerical Investigation of Encapsulated Phase Change Materials Melting Process *via* Enthalpy-Porosity Approach, *Iran. J. Chem. Chem. Eng. (IJCCE)*, **42(7):** 2275-2285 (2022).

[3] Chegenizadeh N., Saeedi A., Xie Q., Application of Nanotechnology for Enhancing Oil Recovery-A Review, *Petroleum*, **2(4)**: 324-333 (2016).

[4] Aziz H., Tunio S.Q., Enhancing Oil Recovery Using Nanoparticles-A Review, *Adv. Nat. Sci.: Nanosci. Nanotechnol.*, **10(3):** 033001 (2019).

[5] Kamal M.S., Adewunmi A.A., Sultan A.S., Al-Hamed M.F., Mehmood U., Recent Advances in Nanoparticles Enhanced Oil Recovery: Rheology, Interfacial Tension, Oil Recovery, and Wettability Alteration, *J. Nanomater.*, **2017:** 2473175 (2017).

[6] Ali J.A., Kolo K., Manshad A.K., Mohammadi A.H., Recent Advances in Application of Nanotechnology in Chemical Enhanced Oil Recovery: Effects of Nanoparticles on Wettability Alteration, Interfacial Tension Reduction, and Flooding, *Egypt. J. Pet.*, **27(4):** 1371-1383 (2018).

[7] Khoramian R., Ramazani A., Hekmatzadeh M., Kharrat R., Asadian E., Graphene Oxide Nanosheets for Oil Recovery, *ACS Appl. Nano Mater.*, **2(9):** 5730-5742 (2019).

[8] Mohajeri M., Hemmati M., Shekarabi A.S., An Experimental Study on Using a Nanosurfactant in an EOR Process of Heavy Oil in a Fractured Micromodel, *J. Pet. Sci. Eng.*, **126:** 162-173 (2015).

[9] Tavakkoli O., Kamyab H., Junin R., Ashokkumar V., Shariati A., Mohamed A.M., SDS-Aluminum Oxide Nanofluid for Enhanced Oil Recovery: IFT, Adsorption, and Oil Displacement Efficiency, *ACS Omega*, **7(16):** 14022-14030 (2022).

[10] Kazemzadeh Y., Sharifi M., Riazi M., Rezvani H., Tabaei M., Potential Effects of Metal Oxide/SiO_2 Nanocomposites in EOR Processes at Different Pressures, *Col. Sur. Ph. Eng. Asp.*, **559:** 372-384 (2018).

[11] Garmroudi A., Kheirollahi M., Mousavi S.A., Fattahi M., Mahvelati E.H., Effects of Graphene Oxide/TiO_2 Nanocomposite, Graphene Oxide Nanosheets and Cedr Extraction Solution on IFT Reduction and Ultimate Oil Recovery from a Carbonated Rock, *Petroleum*, **8(4):** 476-482 (2022).

[12] Omidi A., Manshad A.K., Moradi S., Ali J.A., Sajadi S.M., Keshavarz A., Smart- and Nano-Hybrid Chemical EOR Flooding Using Fe_3O_4/Eggshell Nanocomposites, *J. Mol. Liq.*, **316:** 113880 (2020).

[13] Nourinia A., Manshad A.K., Shadizadeh S.R., Ali J.A., Iglauer S., Keshavarz A., Mohammadi A.H., Ali M., Synergistic Efficiency of Zinc Oxide/Montmorillonite Nanocomposites and a New Derived Saponin in Liquid/Liquid/Solid Interface-Included Systems: Application in Nanotechnology-Assisted Enhanced Oil Recovery, *ACS Omega*, **7(29):** 24951-24972 (2022).

[14] Asl F.O., Zargar G., Manshad A.K., Iglauer S., Keshavarz A., Experimental Investigation and Simulation for Hybrid of Nanocomposite and Surfactant as EOR Process in Carbonate Oil Reservoirs, *Fuel*, **319:** 123591 (2022).

[15] Jafari S., Sillanpää M., Adsorption of Dyes onto Modified Titanium Dioxide, "Advanced Water Treatment", 85-160 Elsevier, Amsterdam, The Netherlands (2020).

[16] Jung M.R., Horgen F.D., Orski S.V., Rodriguez C.V., Beers K.L., Balazs G.H., Jones T.T., Work T.M., Brignac K.C., Royer S., Hyrenbach D., Jensen B.A., Lynch J.M., Validation of ATR FT-IR to Identify Polymers of Plastic Marine Debris, Including Those Ingested by Marine Organisms, *Mar. Pollut. Bull.*, **127:** 704-716 (2018).

[17] Khalil M.W., Eldin T.A.S., Hassan H.B., El-Sayed K., Hamid Z.A., Electrodeposition of Ni–GNS–TiO_2 Nanocomposite Coatings as Anticorrosion Film for Mild Steel in Neutral Environment, *Surf. Coat. Technol.*, **275:** 98-111 (2015).

[18] Dong S., Dou X., Mohan D., Pittman C.U., Luo J., Synthesis of Graphene Oxide/Schwertmannite Nanocomposites and Their Application in Sb(V) Adsorption from Water, *Chem. Eng. J.*, **270:** 205-214 (2015).

[19] Wei X., Li Q., Hao H., Yang H., Li Y., Sun T., Li X., Preparation, Physicochemical and Preservation Properties of Ti/ZnO/In Situ SiOx Chitosan Composite Coatings, *J. Sci. Food Agric.*, **100(2):** 570-577 (2020).

[20] Liu X., Wang X., Li J., Wang X., Ozonated Graphene Oxides as High Efficient Sorbents for Sr(II) and U(VI) Removal from Aqueous Solutions, *Sci. China Chem.*, **59:** 869-877 (2016).

[21] Mohan S., Kumar V., Singh D.K., Hasan S.H., Effective Removal of Lead Ions Using Graphene Oxide-MgO Nanohybrid from Aqueous Solution: Isotherm Kinetic and Thermodynamic Modeling of Adsorption, *J. Environ. Chem. Eng.*, **5(3):** 2259-2273 (2017).

[22] Shahmoradi A.R., Talebibahmanbigloo N., Nickhil C., Nisha R., Javidparvar A.A., Ghahremani P., Bahlakeh G., Ramezanzadeh B., Molecular-MD/Atomic-DFT Theoretical and Experimental Studies on the Quince Seed Extract Corrosion Inhibition Performance on the Acidic-Solution Attack of Mild-Steel, *J. Mol. Liq.*, **346:** 117921 (2022).

[23] Lushinga N., Cao L., Dong Z., Effect of Silicone Oil on Dispersion and Low-Temperature Fracture Performance of Crumb Rubber Asphalt, *Adv. Mater. Sci. Eng.*, **2019:** 8602562 (2019).

[24] Sethy N., Arif Z., Mishra P.K., Kumar P., Synthesis of SiO_2 Nanoparticle from Bamboo Leaf and Its Incorporation in PDMS Membrane to Enhance Its Separation Properties, *J. Polym. Eng.*, **39(7):** 679-687 (2019).

[25] Rocha Segundo I.G.D., Dias E.A.L., Fernandes F.D.P., Freitas E.F.D., Costa M.F., Carneiro J.O., Photocatalytic Asphalt Pavement: The Physicochemical and Rheological Impact of TiO_2 Nano/Microparticles and ZnO Microparticles onto the Bitumen, *Road Mater. Pavement Des.*, **20(6):** 1452-1467 (2019).

[26] Bineesh K.V., Kim D.K., Park D.W., Synthesis and Characterization of Zirconium-Doped Mesoporous Nano-Crystalline TiO_2, *Nanoscale*, **2(7):** 1222-1228 (2010).

[27] Yu H., Zhang B., Bulin C., Li R., Xiang R., High-efficient Synthesis of Graphene Oxide Based on Improved Hummers Method, *Sci. Rep.*, **6:** 36143 (2016).

[28] Sharifi Z., Pakshir M., Amini A., Rafiei R., Hybrid Graphene Oxide Decoration and Water-Based Polymers for Mild Steel Surface Protection in Saline Environment, *J. Ind. Eng. Chem.*, **74:** 41-54 (2019).

[29] Ramezanzadeh M., Ramezanzadeh B., Mahdavian M., Bahlakeh G., Development of Metal-Organic Framework (MOF) Decorated Graphene Oxide Nanoplatforms for Anti-Corrosion Epoxy Coatings, *Carbon*, **161:** 231-251 (2020).

[30] Ma Y., Di H., Yu Z., Liang L., Lv L., Pan Y., Zhang Y., Yin D., Fabrication of Silica-Decorated Graphene Oxide Nanohybrids and the Properties of Composite Epoxy Coatings Research, *Appl. Surf. Sci.*, **360:** 936-945 (2016).

[31] Sun J., Xu Z., Li W., Shen X., Effect of Nano-SiO_2 on the Early Hydration of Alite-Sulphoaluminate Cement, *Nanomaterials*, **7(5):** 102 (2017).

[32] Liang Y., Ouyang J., Wang H., Wang W., Chui P., Sun K., Synthesis and Characterization of Core-Shell Structured SiO_2@YVO_4:Yb^{3+}, Er^{3+} Microspheres, *Appl. Surf. Sci.*, **258(8):** 3689-3694 (2012).

[33] Iatridi Z., Evangelatou K., Theodorakis N., Angelopoulou A., Avgoustakis K., Tsitsilianis C., Multicompartmental Mesoporous Silica/Polymer Nanostructured Hybrids: Design Capabilities by Integrating Linear and Star-Shaped Block Copolymers, *Polymers*, **12(1):** 51 (2020).

[34] Massard C., Bourdeaux D., Raspal V., Feschet-Chassot E., Sibaud Y., Caudron E., Devers T., Awitor K.O., One-pot Synthesis of TiO_2 Nanoparticles in Suspensions for Quantification of Titanium Debris Release in Biological Liquids, *Adv. Nano.*, **1(3):** 86-94 (2012).

[35] Suresh K., Yusoff F., Thermal Stability and Porosity of Reduced Graphene Oxide/Zinc Oxide Nanoparticles and Their Capacity as a Potential Oxygen Reduction Electrocatalyst, *Malaysian J. Anal. Sci.*, **24(3):** 405-412 (2020).

[36] Vallejo W., Rueda A., Diaz-Uribe C., Grande C., Quintana P., Photocatalytic Activity of Graphene Oxide–TiO_2 Thin Films Sensitized by Natural Dyes Extracted from *Bactris Guineensis*, *R. Soc. Open Sci.*, **6(3):** 181824 (2019).

[37] Haeri S.Z., Ramezanzadeh B., Asghari M., A Novel Fabrication of a High Performance SiO_2-Graphene Oxide (GO) Nanohybrids: Characterization of Thermal Properties of Epoxy Nanocomposites Filled with SiO_2-GO Nanohybrids, *J. Col. Int. Sci.*, **493:** 111-122 (2017).

[38] Ramezanzadeh B., Haeri Z., Ramezanzadeh M., A Facile Route of Making Silica Nanoparticles-Covered Graphene Oxide Nanohybrids (SiO_2-GO); Fabrication of SiO_2-GO/Epoxy Composite Coating with Superior Barrier and Corrosion Protection Performance, *Chem. Eng. J.*, **303:** 511-528 (2016).

[39] Sharma T., Sangwai J.S., Silica Nanofluids in Polyacrylamide with and without Surfactant: Viscosity, Surface Tension, and Interfacial Tension with Liquid Paraffin, *J. Pet. Sci. Eng.*, **152:** 575-585 (2017).

[40] Ahmadi M., Chen Z., Challenges and Future of Chemical Assisted Heavy Oil Recovery Processes, *Adv. Colloid Interface Sci.*, **275:** 102081 (2020).